ELSEVIER

Polymer 40 (1999) 3515–3523

polymer

Time-resolved X-ray studies of structure development in poly(butylene terephthalate) during isothermal crystallization

Benjamin S. Hsiao[a,*], Zhi-gang Wang[a], Fengji Yeh[a], Yan Gao[b], Kapil C. Sheth[b]

[a]*Department of Chemistry, State University of New York at Stony Brook, Stony Brook, NY 11794-3400, USA*
[b]*Corporate Research and Development, General Electric Company, Schenectady, NY 12309, USA*

Received 30 March 1998; received in revised form 18 July 1998; accepted 28 July 1998

Abstract

Isothermal melt crystallization in poly(butylene terephthalate) (PBT) homopolymers and glass-fiber-filled composite was studied by time-resolved simultaneous small- and wide-angle X-ray scattering (SWAXS) methods using synchrotron radiation. During primary crystallization, both average long period and lamellar thickness exhibit a significant decrease. During secondary crystallization, the long period and lamellar thickness show a smaller decrease over a longer period of time, which is approximately linear with log time. Similar to other semicrystalline polymers, the morphology of PBT formed during isothermal crystallization can be best described by a dual-lamellar stack model. In this model, primary lamellar stacks are formed first comprising thicker crystalline lamellae, whereas secondary lamellar stacks are formed later *between* the primary lamellar stacks (as observed by the small change of the interlayer amorphous thickness with time). In addition, no isothermal lamellar thickening is observed. From SWAXS measurements, the appearance of the SAXS peak appears to occur prior to WAXD crystal reflection peaks, suggesting that density fluctuations are probably present before melt crystallization. The lamellar morphology and crystallization rate is found to be a function of molecular weight. The glass filler in the PBT composites has no obvious effect on the lamellar structure, but it appears to act as a nucleating agent.

Keywords: Isothermal melt crystallization; PBT; SWAXS

1. Introduction

Poly(butylene terephthalate), PBT, is a commercially important engineering polymer with a wide range of applications such as injection molding and extrusion. As a member of the polyester family, it is also often used as the matrix material in glass fiber reinforced composites, having attractive mechanical properties, good moldability and fast crystallization rate. PBT has some processing advantages over its chemical relative, poly(ethylene terephthalate), PET [1–3]. The melting temperature of PBT is about 230°C, which is lower than PET, (ca. 270°C), allowing PBT to be processed at lower temperatures [4]. In addition, PBT has a lower glass transition temperature, a faster crystallization rate, and approximately the same achievable maximum crystallinity as compared to PET.

Physical properties and morphology in PBT have been studied by a variety of methods, though not as extensively as PET. For example, morphologies of normal and anomalous PBT spherulites with different extinction patterns have been investigated using optical microscopy, small-angle light scattering, and transmission electron microscopy [5–9]. Relaxation mechanisms have been investigated by nuclear magnetic resonance (NMR) [10,11]. Thermal [12,13], mechanical [14,15], and electrical properties [16,17] have also been reported. The crystal structure in PBT was determined by wide-angle X-ray diffraction (WAXD) and further investigated by small-angle X-ray scattering (SAXS) [18–21], infrared [22,23], Raman [24,25], and NMR [26]. Two crystalline modifications, α and β forms, were found in the triclinic crystal unit cells. The β form occurs only under special processing conditions, such as application of stress to the unoriented crystal (transformation between the α form and the β form is reversible) [14,19].

All SAXS and WAXD studies mentioned above were performed using conventional X-ray sources. Recently, real-time SAXS and WAXD methods using synchrotron radiation have been applied to study the thermal expansion of PBT with temperature from 35°C to 235°C [27]. Simultaneous SAXS and WAXD methods have also been performed to investigate the melting, reaction and

* Corresponding author.

0032-3861/99/$ - see front matter
PII: S0032-3861(98)00573-4

recrystallization behavior in a reactive PC–PBT blend [28]. In this study, our objective is to follow the structure development of PBT during isothermal crystallization using time-resolved SWAXS techniques to explore the early stage of primary crystallization and the late stage of secondary crystallization. Similar studies in PET [29] and PEEK [30–33] have been carried out which provided several new insights into the behavior of polymer crystallization. In this work, two PBT homopolymers with different molecular weights and one PBT composite with 30% glass fiber filler were chosen to further examine the effects of molecular weight and glass filler on the morphological development at the lamellar level.

2. Experimental section

PBT samples under the trade name of Valox®195, Valox®315 and Valox®420 were provided by GE Plastics. The weight-average molecular weights M_w of Valox®195 and Valox®315 are 45 000 and 105 000, respectively. The M_w of Valox®420 (30% glass fiber filled) may be lower than its starting compound (Valox®315), since mixing can induce a transesterification process and lower the molecular weight. All the samples exhibit a melting point at 221–225°C and a glass temperature at 40–45°C. The polydispersity (M_w/M_n) in these samples is about 2.

Simultaneous WAXD and SAXS profiles were recorded using two Braun linear position sensitive detectors (PSD) at the Advanced Polymer Beamline (X27C) of the National Synchrotron Light Source (NSLS), Brookhaven National Laboratory (BNL). The wavelength of the X-rays, λ, was 1.307 Å, which was defined by a double multi-layer monochromator. The synchrotron X-rays were collimated with a three pinhole device [34]. Several data acquisition times were used: 5, 10 or 20 s (depending on the crystallization rate). The sample to detector distance for the SAXS measurement is 1715 mm. The angular range for the WAXD measurement is $8° < 2\theta < 39°$.

A dual-chamber temperature jump unit was used for isothermal crystallization measurement. Detailed description of this apparatus has been provided previously [30,35]. Briefly, in melt crystallization study, the PBT sample was first equilibrated at 260°C for 5 min in one chamber and pneumatically 'jumped' to a second chamber (aligned in the path of the X-ray beam) for time-resolved crystallization measurement. The chosen crystallization temperatures are 50, 90, 130, 170, 190, 195 and 200°C. The transition time to reach the temperature equilibrium after the jump is 30–90 s. In most cases, the initial 90% of the temperature change had a rate about 300°C/min. At the thermal equilibrium, the fluctuation in temperature was usually less than ± 0.5°C.

2.1. SAXS data analysis

The SAXS profile was analyzed via a combination of correlation $\gamma(r)$ and interface distribution function $g(r)$ methods [36,37]:

$$\gamma(r) = \left(\int_0^\infty I(q)\cos(qr)\mathrm{d}q\right)/Q \tag{1}$$

$$g(r) = \partial^2(\gamma(r))/\partial r^2 = -\left(\int_0^\infty I(q)q^2\cos(qr)\mathrm{d}q\right)/Q. \tag{2}$$

Here q is the scattering vector ($q = [2\pi/\lambda]\sin(2\theta)$, where 2θ is the scattering angle), $I(q)$ is the scattering intensity after the Lorentz correction and Q is the invariant. The correlation function is the Fourier transform of the Lorentz corrected SAXS profile. The interface distribution function $g(r)$ is the Fourier transform of the interference function $G(q)$ [36]:

$$g(r) = \int_0^\infty G(q)\cos(qr)\mathrm{d}q. \tag{3}$$

Since the SAXS profile can only be collected in a limited angular range ($0.1\ \mathrm{nm}^{-1} < q < 2.5\ \mathrm{nm}^{-1}$), it must be extrapolated to both high and low q values prior to the Fourier transformation. The extrapolation to the high q values was performed according to Porod's law.

The measured scattering intensity $I_{obs}(q)$ includes contributions from liquid-like 'background' scattering $I_b(q)$ and finite interface between the two constituting phases. The scattering intensity in the Porod region thus becomes [38]:

$$\lim_{q\to\infty} I_{obs}(q) = I_b(q) + (K/q^4)\exp(-\sigma^2q^2) \tag{4}$$

where σ is related to the width of the interface and K is the Porod constant. The exponential term corrects for the contribution from the crystal–amorphous interface. Instead of using the conventional method such as $I_{obs}q^4$ versus q^4 to estimate the contributions of I_b and exponential term [39], the following two criteria based on the interference function were used to obey Porod's law [40]:

$$\lim_{q\to\infty} G(q) = \lim_{q\to\infty}\left[K - (I_{obs}(q) - I_b(q))q^4\exp(\sigma^2q^2)\right] = 0 \tag{5}$$

$$\int_0^\infty G(q)\mathrm{d}q = \int_0^\infty\left[K - (I_{obs}(q) - I_b(q))q^4\exp(\sigma^2q^2)\right]\mathrm{d}q = 0. \tag{6}$$

The second criterion (Eq. (6)) is based on the assumption that the finite transition zone between the two constituting phases has been accounted for and the interface distribution function will start from the origin ($g(0) = 0$). Since $g(r)$ is the Fourier transform of $G(q)$, the total area of $G(q)$ will be zero.

The correlation and interface distribution functions must be interpreted with a suitable morphological model. Herein, we used the finite lamellar stack model, consisting of finite numbers of crystalline lamellae separated by interlamellar amorphous layers in stacks. The long spacing (L_c^M, noted as L from now on) can be estimated as the position of the first maximum in the correlation function. The analysis of the

correlation function using this model yields further information about the average crystal lamellar thickness (l_c), amorphous layer thickness (l_a), and linear crystallinity within the stack χ_{cl} ($= l_c/L$). Note that the analysis of the correlation alone cannot assign the values for l_c and l_a. The justification for our assignment will be discussed later.

2.2. WAXD data analysis

For the WAXD profile, the integrated intensity, peak position, peak height and peak width for each crystal reflection peak were extracted by a custom made curve-fitting program. Two broad Gaussian peaks were used to describe the amorphous background. All other peaks were also fitted with Gaussian functions. By dividing the sum of the crystalline reflection intensities, I_c, to the overall intensity, I_{total} , an estimate of the crystallinity ϕ_{mc} (by weight) was obtained. The true value of crystallinity may be higher because the defects and the thermal distortions in the crystal lattice, and other factors that can cause a reduction of I_c are not accounted for. The apparent crystallinity is related to the actual volume degree of crystallinity, ϕ_{vc}, in the sample by $\phi_{mc} = f(T)\phi_{vc}$, where $f(T)$ is a temperature-dependent factor taking into account the corrections mentioned above and the density conversion from mass to volume.

3. Results and discussion

3.1. PBT homopolymer (Valox®195)

Typical real-time simultaneous SAXS and WAXD profiles recorded during isothermal crystallization of Valox®195 at 195°C are shown in Fig. 1(a) and Fig. 1(b). After the SAXS analysis, the evolution of morphology variables of Valox®195 during isothermal crystallization at 170°C are summarized in Fig. 2 (the total crystallization time was 10 min). Fig. 2(a) illustrates the changes in scattering invariant (Q), long period (L, the position of the first maximum, and L_c^m, twice the position of the first minimum, in the correlation function), crystal lamellar thickness (l_c) and amorphous interlamellar layer thickness (l_a). Fig. 2(b) illustrates the value of Q and the height of the first minimum in the normalized interface distribution function (g_{minh1}/Q). The latter represents the volume fraction of the lamellar stacks. In Fig. 2(a), we assigned the values for l_c to be larger than l_a ($l_1 = l_c$, $l_2 = l_a$). As we will discuss later, this assignment can be justified from the experimental data. The

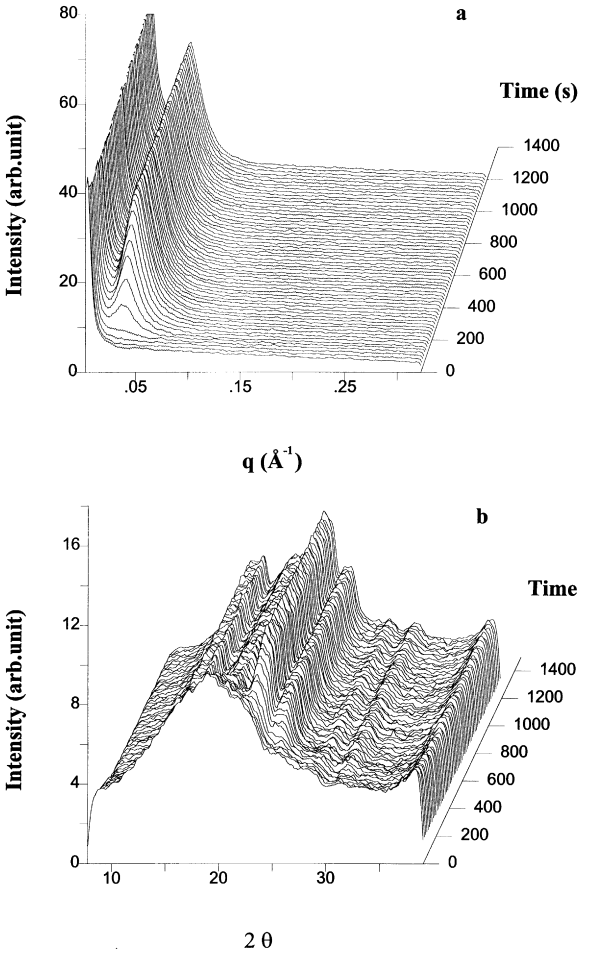

Fig. 1. Time-resolved SAXS (a) and WAXD (b) profiles recorded during isothermal crystallization process of Valox®195 at 195°C.

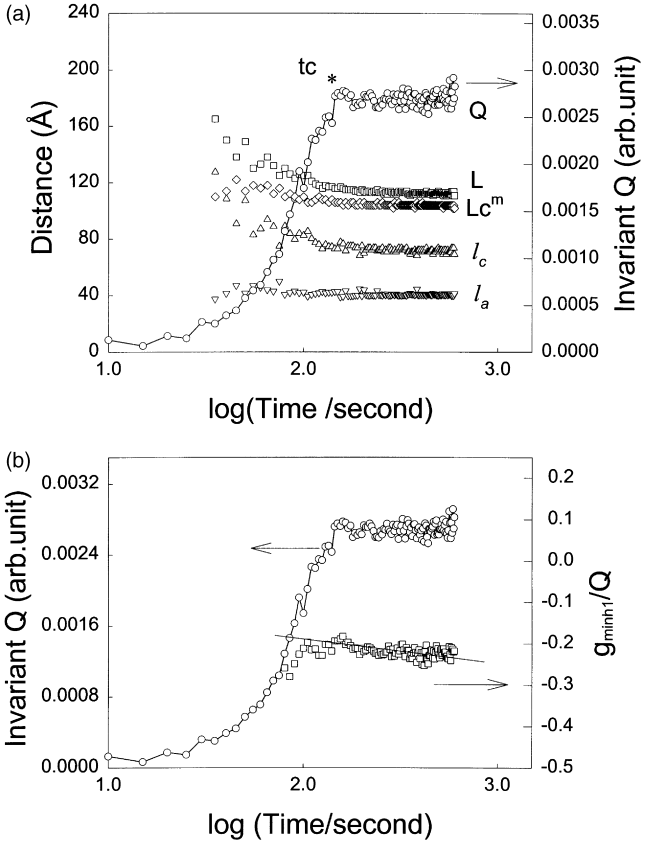

Fig. 2. Morphological variables during isothermal melt crystallization of Valox®195 at 170°C (a) the values of L, L_c^m, l_c, l_a and Q; (b) The height of the first minimum in the normalized interface distribution function (g_{minh1}/Q).

evolution of these variables for the other temperatures (50, 90, 130, 170, 190, 195 and 200°C) is very similar to Fig. 2. For comparison purposes, we have also included Fig. 3(a) and Fig. 3(b) from isothermal crystallization at 130°C.

Several interesting features in the morphological changes during isothermal crystallization of PBT can be found from Figs. 2 and 3: (1) During the initial crystallization stages, the average long period (L and L_c^m) and the average lamellar thickness (l_c) exhibit a significant decrease. We attribute this behavior to the occurrence of the thinner secondary lamellae within (the lamellar insertion model) or between (the stack insertion model) the existing primary lamellar stacks (the average values of L and l_c decrease as the secondary lamellae increase) [30,33,35,41,42]. Since the change in l_a is relatively small, we favor the stack insertion model for secondary crystallization. We have defined the primary crystallization dominant stage as the regime ($t < tc$, note the symbol * in Fig. 2(a)) during which the invariant Q exhibits a sigmoidal increase with log time. In PEEK samples, calorimetric study indicated that this regime corresponds to the development of the high endotherm [43]. Since multiple melting endotherms have also been observed in PBT upon isothermal annealing [44,45], we believe the same mechanism applies. (2) At the later crystallization stage, the long period and lamellar thickness exhibit a smaller decay over a longer period of time, which is approximately linear with log time. We attribute this stage to the secondary crystallization stage where the event of forming thinner secondary lamellae dominates. (3) During secondary crystallization, the magnitude of the first minimum in the normalized interface distribution function increases (absolute value decreases) linearly with log time (Fig. 2(b) and Fig. 3(b)). On the basis of this observation, it can be concluded that the amount of secondary lamellar stacks increases linearly with log time.

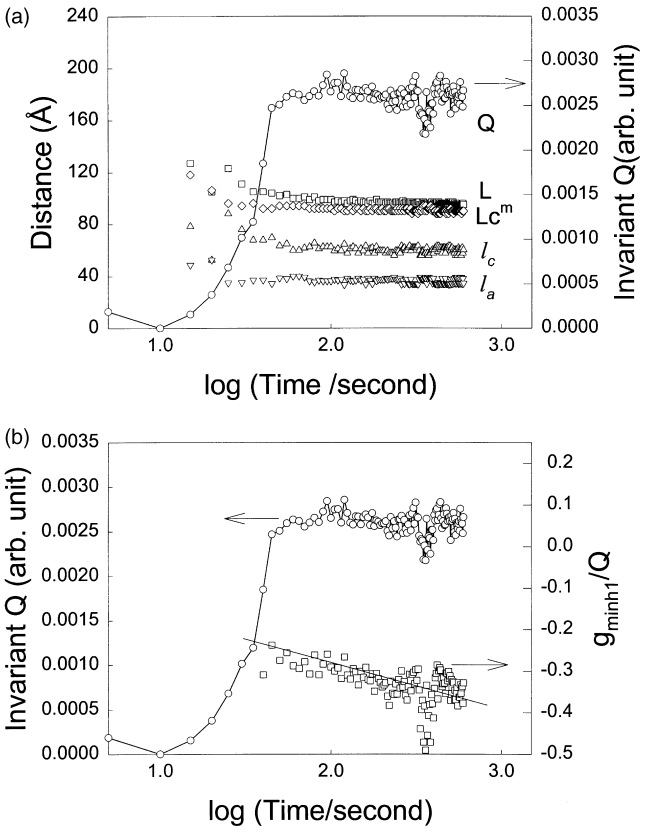

Fig. 3. Morphological variables during isothermal melt crystallization of Valox®195 at 130°C (a) The values of L, L_c^m, l_c, l_a and Q; (b) The height of the first minimum in the normalized interface distribution function (g_{minh1}/Q).

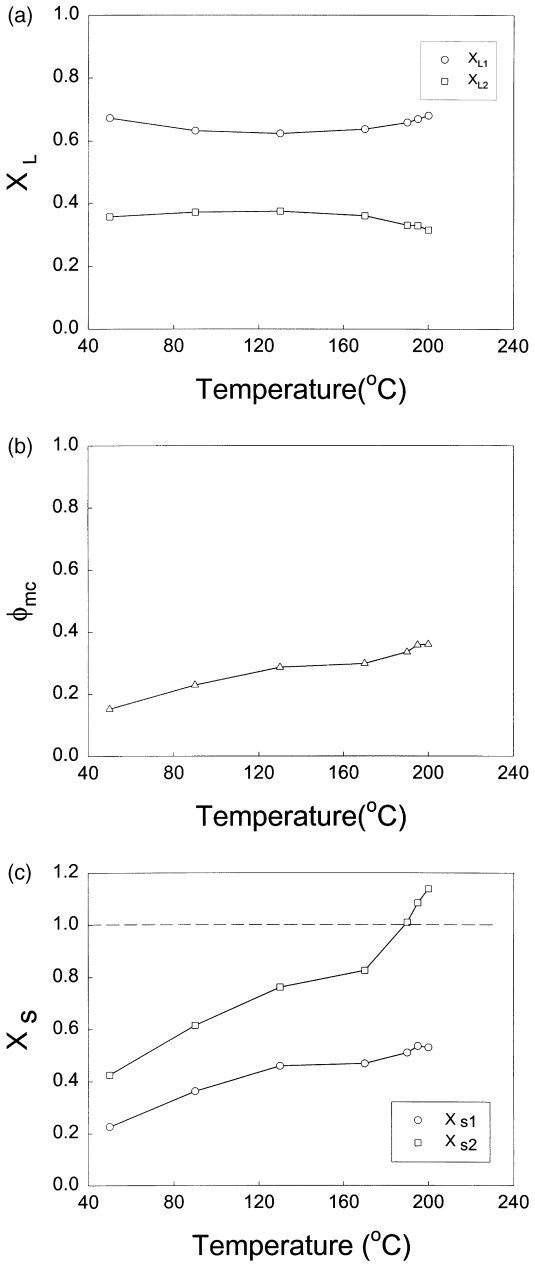

Fig. 4. (a) The linear degree of crystallinity within the lamellar stacks (χ_{L1} ($=l_1/L$) and χ_{L2} ($=l_2/L$)); (b) The mass fraction crystallinity ϕ_{mc} from WAXD; (c) The volume fraction of lamellar stacks in the bulk sample (χ_{S1} ($=\phi_{mc}/\chi_{L1}$) or χ_{S2} ($=\phi_{mc}/\chi_{L2}$)) as a function of temperature for Valox®195.

At this point, we would like to acknowledge the uncertainty of the correlation function analysis. Briefly, the analysis can yield an average long period, and two average values for crystal lamellar and amorphous interlayer thicknesses [46]. However, the correlation function method cannot distinguish which value represents which thickness. As stated previously, we select the larger value as the crystal thickness. Our reasons can be demonstrated in Fig. 4(a–c). In Fig. 4(a), we use the plateau values of L, l_1 and l_2 (invariant with time at the late stage of crystallization) for the justification, and consider two situations: either χ_{L1} ($= l_1/L$) or χ_{L2} ($= l_2/L$) will represent the linear degree of crystallinity within the lamellar stacks. In Fig. 4(b), ϕ_{mc} is the mass degree of crystallinity determined from WAXD. We can then define χ_{S1} ($= \phi_{mc}/\chi_{L1}$) or χ_{S2} ($= \phi_{mc}/\chi_{L2}$) as the volume fraction of the lamellar stacks in the bulk sample (Fig. 4(c)). The small difference between the densities of amorphous PBT ($\sim$1.28 g/cm^3) and crystalline PBT ($\sim$1.32 g/cm^3) [6] suggests that a minor correction to translate the mass to the volume degree of crystallinity may be ignored. Historically, most authors assumed that the lamellar thickness could be estimated by multiplying the long period and the overall degree of crystallinity [27,31,32,47,48]. Such an approach precludes the existence of amorphous-rich interstack regions. As a result, the value of χ_{L2} (local fraction) must be approximately equal to ϕ_{mc} (bulk fraction), i.e. the volume fraction of lamellar stacks χ_S should be 1. However, in Fig. 4(c), at temperatures of 200°C, 195°C and 190°C, we found the values of χ_{S2} to be larger than 1, which are not physically meaningful. With the other assignment, the computed value for χ_{S1} is always less than unity. This can be understood by the presence of non-crystallized materials outside the lamellar stacks (the value of χ_{L1} becomes larger than ϕ_{mc}). Furthermore, the observations of decreasing trend in χ_{L2} and the increasing trend in χ_{L1} (except the data at 50°C) with temperature are also against the assignment of l_2 as the lamellar thickness (since the crystal thickness is expected to increase with temperature).

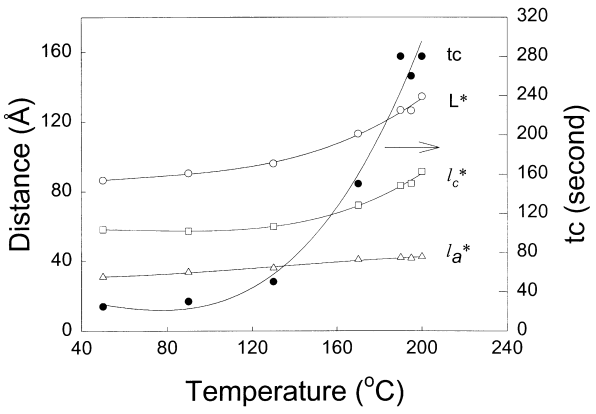

Fig. 5. The variation of morphological variables (L*, l_c* and l_a*) and tc (the time when the primary crystallization is completed) at different temperatures for Valox®195.

There are other interesting morphological changes observed during isothermal crystallization. First, we note that L does not correspond to L_c^m (Fig. 2(a), Fig. 3(a)). Similar observations have been made previously in PET [49]. The model calculations by Santa-Cruz et al. [50] and our laboratory suggest that as $L > L_c^m$, it implies that the thicker phase has a broader distribution of sizes than the thinner phase. In this case, the thicker phase corresponds to the crystalline lamellar phase, and the amorphous layer thickness is characterized by a narrower distribution of the thickness. The difference between L and L_c^m gradually decreases when the crystallization temperature decreases (as seen in Fig. 2(a), Fig. 3(a)), which indicates that the distribution of the lamellar thickness becomes narrower as the crystallization temperature decreases. This may be reasonable as we expect the primary lamellar thickness and the secondary lamellar thickness to approach each other at a high degree of supercooling. Second, we define a characteristic time (tc) during isothermal crystallization (when the values of Q, L, l_1 and l_2 reach the plateau region), which can be viewed as the time when the primary crystallization stage is completed. The values of tc at different crystallization temperatures are shown in Fig. 5. At low temperatures (50°C and 90°C), the value of tc is short, indicating that the primary crystallization process is fast. At high temperatures, tc is seen to increase significantly, indicating that longer time is needed for primary crystallization as expected. In Fig. 5, both final values of long period (L*) and lamellar thickness (l_c*), are found to increase with temperature, whereas the final thickness of the amorphous interlayer (l_a*) only has a slight increase.

We now turn our attention to the change of the apparent crystallinity with temperature for this polymer. The peak-fitting curves for deconvoluting the WAXD profile are

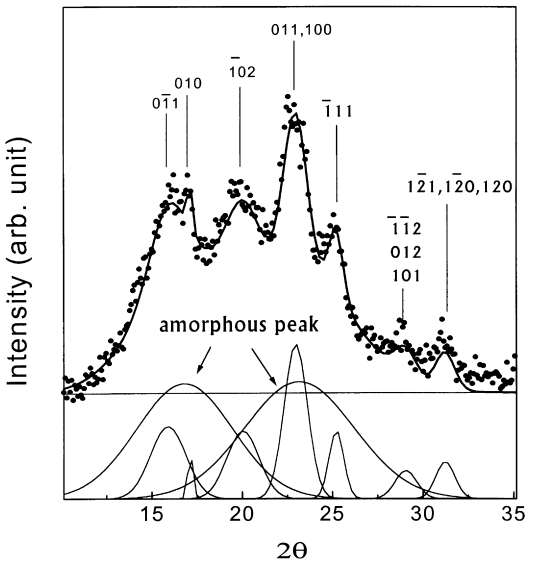

Fig. 6. Illustration of the deconvolution procedure for the WAXD profile (Valox®195 crystallized at 190°C for 20 min, two broad peaks represent the amorphous fraction). The Miller indices of the WAXD reflections are also indicated.

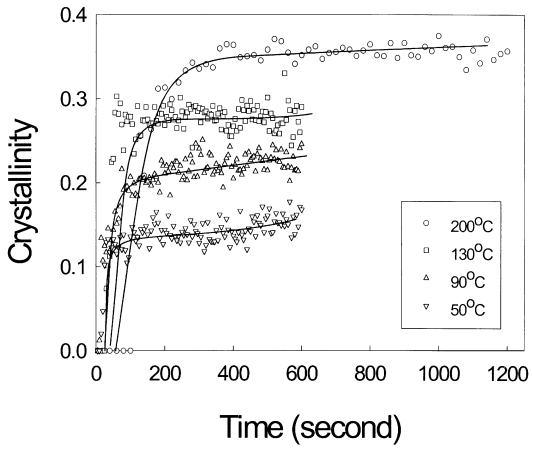

Fig. 7. Evolution of the apparent mass degree of crystallinity (ϕ_{mc}) during isothermal process at different temperatures for Valox®195.

illustrated in Fig. 6. From this analysis, the evolution of the apparent mass degree of crystallinity, ϕ_{mc}, can be estimated (Fig. 7). In this figure, large signal fluctuations in ϕ_{mc} are seen, which are due to the relatively low diffraction intensity collected using a short acquisition time. The final ϕ_{mc} as a function of temperature has also been shown in Fig. 4(b). This result is in good agreement with that in [6], where the mass percent crystallinity is obtained by density measurement. The slight increase of ϕ_{mc} by the crystallization temperature indicates that crystal lattice perfection is improved. We can also determine the value of *tc* from the ϕ_{mc} profile, which is similar to *tc* determined from SAXS. Since we conclude that no lamellar thickening occurs from the SAXS data, the prolonged isothermal annealing will both improve the crystal lattice perfection in the existing lamellae and generate new (defective) secondary lamellae.

Because the SAXS and WAXD profiles are collected simultaneously, it is interesting to compare the time sequence of the two events. It has been reported that, during isothermal crystallization from the glass state of PET and PEEK samples, the SAXS peak appeared before the WAXD crystalline peaks [51,52]. This suggests that density fluctuations (manifest as SAXS signals) may occur prior to crystallization (manifest as WAXD reflections). Results for this comparison from isothermal crystallization of Valox®195 at 200°C, 195°C and 130°C are shown in Figs 8–10, respectively. In these figures, only the time-resolved SAXS and WAXD raw data profiles at the initial stage of crystallization are plotted. It is seen that at 200°C, 195°C and 130°C, the identifiable SAXS peaks appear at 80 s, 60 s and 15 s, respectively, but the WAXD crystal reflection peaks appear at 120 s, 100 s and 25 s, respectively. This confirms the notion that density fluctuations probably exist prior to crystallization. Recently, Ryan et al. have drawn the same conclusion from melt crystallization in other polymers [53]. From Figs. 8–10, it is seen that the time lag between the first SAXS peak and the first WAXD peaks at high

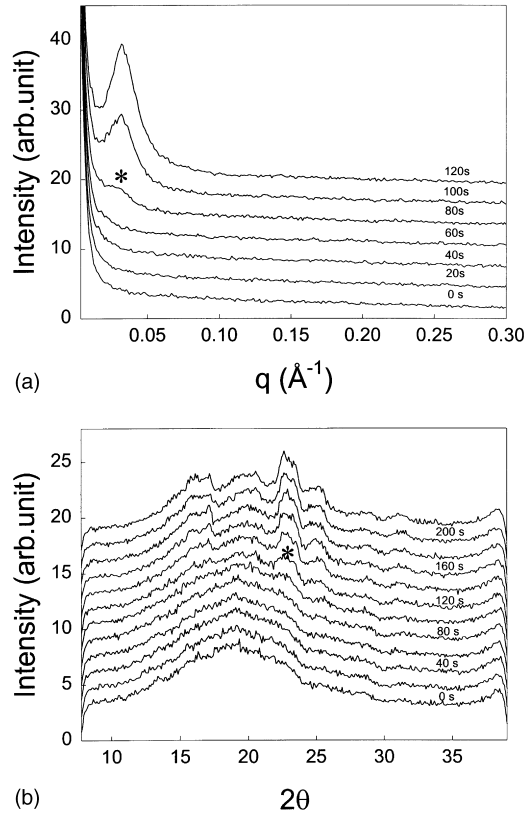

Fig. 8. SAXS (a) and WAXD (b) profiles at the early crystallization stage for Valox®195 at 200°C.

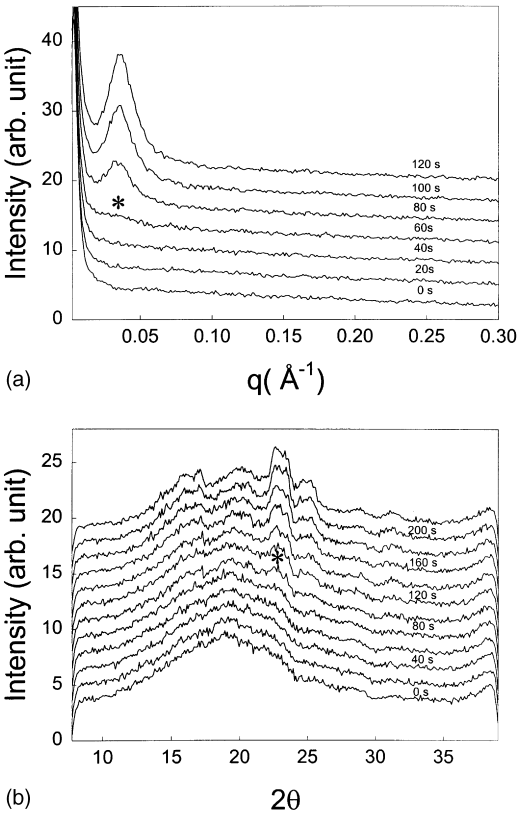

Fig. 9. SAXS (a) and WAXD (b) profiles at the early crystallization stage for Valox®195 at 195°C.

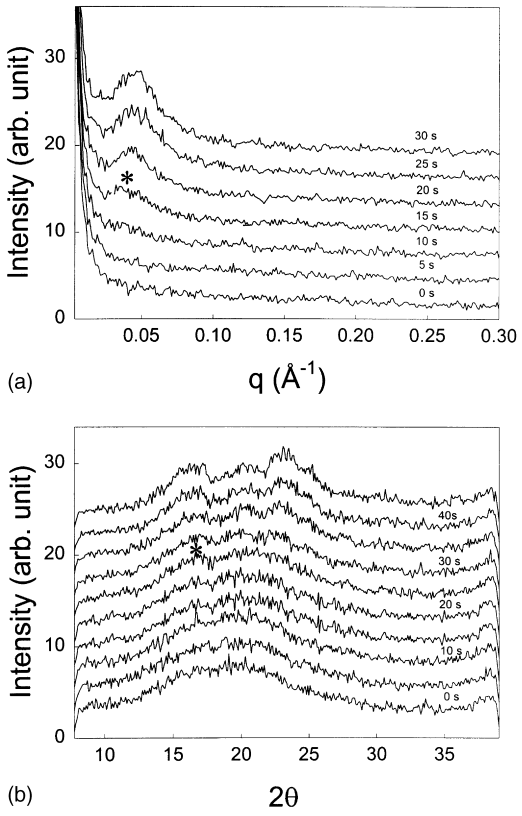

Fig. 10. SAXS (a) and WAXD (b) profiles at the early crystallization stage for Valox®195 at 130°C.

temperature is longer than that at low temperature. So, as we retard the crystallization process by raising the temperature, this enhances the occurrence of density fluctuations in the melt prior to crystallization.

3.2. High M_w PBT homopolymer (Valox®315)

Many physical properties in semicrystalline polymers are functions of crystallization temperature and molecular weight [54,55]. It was also recognized nearly two decades ago that the morphology on the lamellar scale is dependent

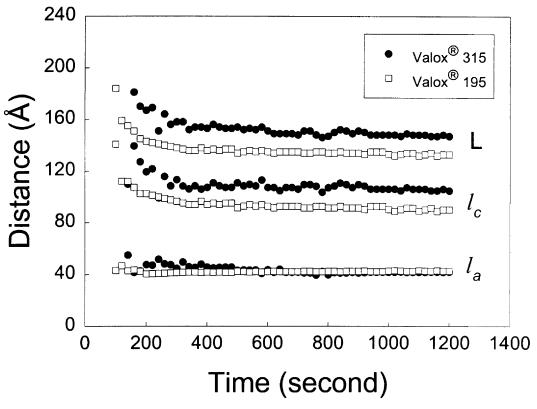

Fig. 11. Time evolution process of L, l_c and l_a for Valox®315 and Valox®195 during isothermal crystallization at 200°C.

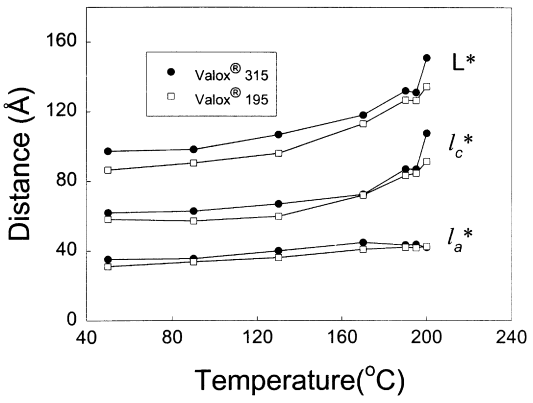

Fig. 12. Morphological variables of L*, l_1* and l_2* for Valox®315 and Valox®195 during isothermal crystallization at different temperatures.

on the molecular weight distribution [56–58]. For example, in monodisperse fractions and mixtures of monodisperse fractions of polyethylene (PE), the long period (from SAXS) is a linear function of the weight average of the dimensions of polymer coils [55,56]. Using electron microscopy, Voight-Martin [57] has also found that the long period in monodisperse PE increases with the molecular weight. In Fig. 11, we compare the time evolution process of L, l_c and l_a for Valox®315 (M_w = 105 000) and Valox®195 (M_w = 45 000) during isothermal crystallization at the same temperature. It is seen that both L and l_c increase when the molecular weight increases, but the value of l_a shows little dependence on the molecular weight. The variation of L*, l_c* and l_a* at the final stage of crystallization with crystallization temperature is shown in Fig. 12. The increases in L* and l_c* seem to be evident, which are consistent with the previous report for different polymers [55–57]. The increase in l_c by M_w may be explained by the following viewpoint. As more entanglements of the chains are encountered in the higher molecular weight sample, longer crystallization time is needed to disentangle the chains for crystallization. As crystallization requires more time to complete (as seen clearly from Fig. 13, where *tc* for Valox®315 is much longer than that for Valox®195), the

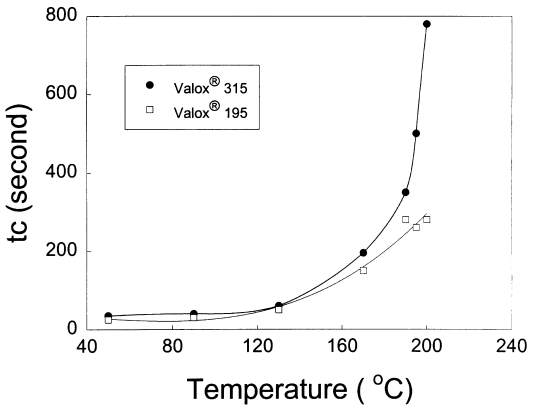

Fig. 13. The value of *tc* of Valox®315 and Valox®195 during isothermal crystallization process at different temperatures.

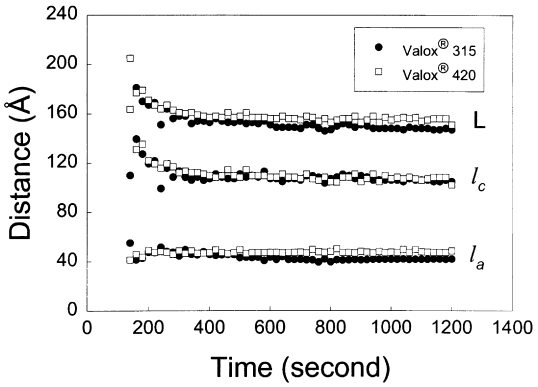

Fig. 14. Time evolution process of L, l_c and l_a for Valox®315 and Valox®420 during isothermal crystallization process at 200°C.

prolonged process can produce a thicker lamellar thickness. We, nevertheless, acknowledge that the M_w effect on morphological parameters in PBT perhaps is not as apparent as the temperature effect. The possibility of transesterification in PBT may also play a role to reduce the M_w effect on the changes of morphological parameters.

3.3. PBT composites with glass fillers (Valox®420)

Generally, PBT is often used with some kinds of glass fillers added as the property enforcing agents. We are thus interested in understanding the effect of glass fillers on the crystal structure development. Fig. 14 shows the resultant morphological variables (L, l_c and l_a) during isothermal crystallization. The sample Valox®420 is the mixture of 30% glass fillers with Valox®315 (as a result, the molecular weight of Valox®420 may be lower than Valox®315 due to the transesterification process during mixing). In Fig. 14, it is seen that the three lamellar parameters of Valox®315 and Valox®420 are very similar to each other. This suggests that the glass filler does not affect the lamellar morphology in PBT, and the molecular weight decrease may be small. The changes of the final average values for L^*, l_c^* and l_a^* are plotted in Fig. 15. Again, no obvious changes in the lamellar

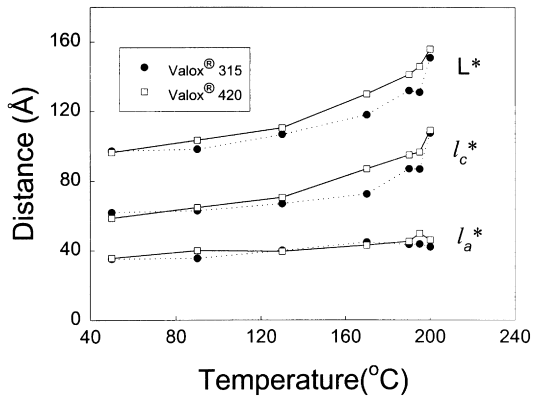

Fig. 15. Morphological variables of L^*, l_1^* and l_2^* for Valox®315 and Valox®420 during isothermal crystallization process at different temperatures.

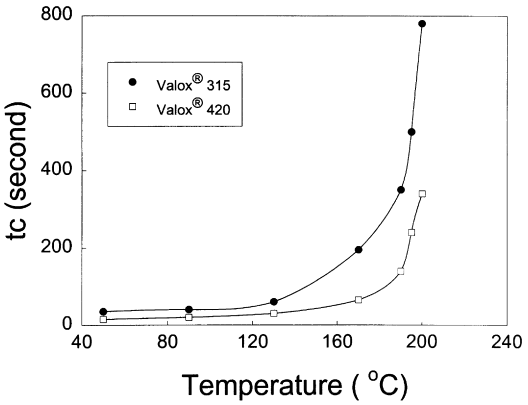

Fig. 16. The value of *tc* of Valox®315 and Valox®420 during isothermal crystallization process at different temperatures.

structure occur when the glass filler is added (except at high temperatures). This phenomenon may be understood by the weak interactions between the PBT matrix and the glass fillers. Because the glass fillers have a very large macrostructure (~1000 nm), they may not impose a direct impact to the formation of the lamellar structure (2–50 nm). Nevertheless, the glass fillers are effective nucleating agents to PBT, which greatly increases the nucleation rate. From the SAXS data, the parameter *tc* as a function of crystallization temperature is shown in Fig. 16. It is seen that *tc* of Valox®420 is much lower than that of Valox®315, which indicates that the primary crystallization process can be completed in a short time with the glass filler added.

4. Conclusions

The following results have been obtained in the present work:

1. Similar to other semicrystalline polymers such as PET and PEEK, the morphology of PBT formed during isothermal crystallization can be best described by a dual-lamellar stack model. Primary lamellar stacks form first and consist of thicker crystalline lamellae. During secondary crystallization, the secondary lamellar stacks probably form *between* the primary lamellar stacks (as observed by the small change in the value of l_a) with thinner long period and lamellar thickness. During this stage, no lamellar thickening occurs.
2. From simultaneous SAXS–WAXD measurements, the appearance of the SAXS peak is seen before WAXD reflection peaks, which suggests that density fluctuations probably exist prior to crystallization.
3. The lamellar morphology appears to be dependent on the molecular weight. Both long period and lamellar thickness increase when the molecular weight increases, but the thickness of interlamellar amorphous layer shows little change with the molecular weight. It is thought that the more entanglements of the chains in the higher

molecular weight sample can increase the crystallization time, leading to a larger lamellar thickness.

4. The glass fillers in PBT composite do not affect the lamellar structure development in the glass-filled PBT composite. However, the glass filler seems to act as a nucleating agent, which increases the crystallization rate.

Acknowledgements

The authors would like to thank financial support of this work in part by the NSF grant (DMR 9732653), and in part by the AP-PRT at the NSLS, BNL and the NSF-GOALI grant (DMR 9629825) for synchrotron measurements. The authors are grateful to Dr. Yajun Wang for providing samples and Drs. Terry Jordan, Sapna Talibudden and Tim Banach (GE CRD) for helpful comments.

References

[1] Gilbert M, Hybart FJ. Polymer 1972;13:327.
[2] Gilbert M, Hybart FJ. Polymer 1974;15:407.
[3] Pratt F, Hobbs SY. Polymer 1976;17:12.
[4] Valero M, Iruin JJ, Espinoza E, Fernandez-Berridi MJ. Polym Comm 1990;31:127.
[5] Misra A, Garg SN. J Polym Sci, Polym Lett Ed 1982;20:121.
[6] Stein RS, Misra A. J Polym Sci, Polym Phys Ed 1980;18:327.
[7] Roche EJ, Stein RS, Thomas EL. J Polym Sci, Polym Phys Ed 1980;18:1145.
[8] Matsuo M, Geshi K, Moriyama A, Sawatari C. Macromolecules 1982;15:193.
[9] Runt J, Du L, Martynowicz LM, Brezny DM, Mayo M. Macromolecules 1989;22:3908.
[10] Perry BC, Koenig JL, Lando JB. Macromolecules 1987;20:422.
[11] Garbow JR, Schaefer J. Macromolecules 1987;20:819.
[12] Cheng SZD, Pan R, Wunderlich B. Makromol Chem 1988;189:2443.
[13] Yeh JT, Runt J. J Polym Sci, Polym Phys Ed 1989;27:1543.
[14] Roebuck J, Jakeways R, Ward IM. Polymer 1992;33:227.
[15] Nakamae K, Kameyama M, Yoshikawa M, Matsunoto T. J Polym Sci, Polym Phys Ed 1982;20:319.
[16] Cerere A, Greco R, Ragosta G, Scarinzi G, Taglialatela A. Polymer 1990;31:1239.
[17] Runt J, Barron A, Zhang X-F, Kumar SK. Macromolecules 1991;24:3466.
[18] Mencil Z. J Polym Sci, Polym Phys Ed 1975;13:2173.
[19] Yokouchi M, Sakakibara Y, Chatani Y, Tadokoro H, Tanaka T, Yoda K. Macromolecules 1976;9:266.
[20] Runt J, Zhang X, Miley DM, Gallagher KP, Zhang A. Macromolecules 1992;25:3902.
[21] Grasso RP, Perry BC, Koenig JL, Lando JB. Macromolecules 1989;22:1267.
[22] Ward IM, Wilding MA. Polymer 1977;18:327.
[23] Dobrovolny-Marand E, Hsu SL, Shih CK. Macromolecules 1987;20:1022.
[24] Bereton MG, Davies GR, Jakeways R, Smith T, Ward IM. Polymer 1978;19:17.
[25] Jakeways R, Smith T, Ward IM, Wilding MA. J Polym Sci, Polym Lett Ed 1976;14:41.
[26] Gomez MA, Cozine MH, Tonelli AE. Macromolecules 1988;21:388.
[27] Hou PT, Cebe P, Capel M. J Polym Sci, B: Polym Phys 1992;30:1459.
[28] Wilkinson AN, Tattum SB, Ryan AJ. Polymer 1997;38:1923.
[29] Jonas AM, Russell TP, Yoon DY. Colloid Polym Sci 1994;272:1344.
[30] Hsiao BS, Gardner KH, Wu DQ, Chu B. Polymer 1993;34 (19):3986.
[31] Fougnies C, Damman P, Dosiere M, Koch MH. Macromolecules 1997;30:1392.
[32] Jonas AM, Russell TP, Yoon DY. Macromolecules 1995;28:8491.
[33] Verma R, Marand H, Hsiao B. Macromolecules 1996;29:7767.
[34] Chu B, Harney P, Li Y, Linhiu K, Ye F, Hsiao B. Rev Sci Instru 1994;65 (3):597.
[35] Hsiao BS., Gardner KH, Wu DQ, Chu B. Polymer 1993;34 (19):3996.
[36] Ruland W. Colloid Polym Sci 1977;255 (5):417.
[37] Stribeck N, Ruland W. J Appl Cryst 1978;11:535.
[38] Koberstein JT, Morra B, Stein RS. J Appl Cryst 1980;13:34.
[39] Balta-Calleja FJ, Vonk GG. X-ray scattering of synthetic polymers. New York: Elsevier Science.
[40] Hsiao BS, Verma RK. J Synchrotron Radiation 1997;5:23.
[41] Verma RK, Hsiao BS. Trends in Polym Sci 1996;4 (9):312.
[42] Kruger K-N, Zachmann HG. Macromolecules 1993;26:5202.
[43] Cheng SZD, Cao MY, Wunderlich B. Macromolecules 1986;19:1868.
[44] Kim J, Nichols ME, Robertson RE. J Polym Sci: Part B: Polym Phys 1994;32:887.
[45] Nichols ME, Robertson RE. J Polym Sci: Part B: Polym Phys 1992;30:755.
[46] Strobl GR, Schneider M. J Polym Sci, Polym Phys Ed 1980;18:1343.
[47] Fougnies C, Damman P, Villers D, Dosiere M, Koch MH. Macromolecules 1997;30:1385.
[48] Lee Y, Porter RS. Macromolecules 1987;20:1336.
[49] Gehrke R, Riekel C, Zachmann HG. Polymer 1989;30:1582.
[50] Santa-Cruz C, Stribeck N, Zachmann HG, Calleja FJB. Macromolecules 1991;24:5980.
[51] Imai M, Mori K, Mizukami T, Kaji K, Kanaya T. Polymer 1992;33:4451.
[52] Ezquerra TA, Lopez-Cabarcos E, Hsiao BS, Balta-Calleja FJ. Phys Rev E Brief Rep 1997.
[53] Ryan AJ, Terrill NJ, Fairclough JPA. ACS PMSE Prep 1998, in press.
[54] Mandelkern L. Crystallization of polymer. New York: McGraw–Hill, 1964.
[55] Mandelkern L. Faraday Discuss Chem Soc 1979;68:310.
[56] Robelin-Souffache E, Rault J. J Phy (Les Ulis, Fr) 1980;41:1459.
[57] Voight-Martin IG. Macromolecules 1984;17:321.
[58] Wunderlich B. Macromolecular physics, vol 2. New York: Academic Press, 1976.